# The MemoFlex II, a non-robotic approach to follow-the-leader motion of a snake-like instrument for surgery using four predetermined physical tracks

Henselmans, P. W.J.; Culmone, C.; Jager, D. J.; van Starkenburg, R. I.B.; Breedveld, P.

**DOI**
10.1016/j.medengphy.2020.10.013

**Publication date**
2020

**Document Version**
Accepted author manuscript

**Published in**
Medical Engineering and Physics

# The MemoFlex II, a non-robotic approach to follow-the-leader motion of a snake-like instrument for surgery using four predetermined physical tracks

P.W.J. Henselmans*[1], C. Culmone*[2], D.J. Jager#[3], R.I.B. van Starkenburg#[4], P. Breedveld*[5]

## Abstract

The fields of Minimally Invasive Surgery (MIS) and Natural Orifices Transluminal Endoscopic Surgery (NOTES) strive to reduce the level of invasiveness by entering the body through smaller incisions and natural orifices. Hyper-redundant snake-like instruments can help in this pursuit of reducing invasiveness. Such instruments can pass along multi-curved pathways through the body without any support or guidance from its anatomical environment. In this way, the width of the surgical pathway and thus the invasiveness of the procedure can be reduced significantly. This is referred to as Follow-the-Leader (FTL) motion.

Generally, surgical instruments intended for FTL-motion are robotic systems that require medical grade actuators, sensors, and controllers, driving up costs and increasing their footprint in the operation room. Our goal was to discard the need for these elements and develop a non-robotic instrument capable of FTL-motion along pre-determined paths. A proof of concept prototype called MemoFlex II was developed, consisting of a cable-driven hyper-redundant shaft that is controlled via four physical tracks. The MemoFlex II was able to perform 3D FTL-motion along pre-determined paths. Among other things, this study reports on a Ø8 mm shaft containing seven

* Faculty Mechanical, Maritime and Materials Engineering, Dept. Biomechanical Engineering, Delft University of Technology, Mekelweg 2, 2628 CD, Delft, the Netherlands
# Dienst Elektronische en Mechanische Ontwikkeling, Delft University of Technology, Mekelweg 4, 2628 CD, Delft, the Netherlands
[1] p.w.j.henselmans@tudelft.nl
[2] c.culmone@tudelft.nl
[3] d.j.jager@tudelft.nl
[4] r.i.b.vanstarkenburg@tudelft.nl
[5] p.breedveld@tudelft.nl

segments and 14 degrees of freedom (DOFs) following several multi-curved paths with an average maximal footprint between 11,0 and 17,1 mm.

***Keywords:*** *Medical Devices, Hyper-Redundant, Snake-Like, Follow-the-Leader, Pathway Surgery, Minimally Invasive Surgery, Natural Orifice Transluminal Endoscopic Surgery*

## 1 Introduction

The field of Natural Orifice Transluminal Endoscopic Surgery (NOTES) strives to reduce the invasiveness of surgery by using the body's natural orifices as the surgical entry-point (1), for example by entering the mouth to reach the stomach through the esophagus, or by entering the nose to reach the skull base through the nasal cavity (2-4). In such cases, a straight pathway from entry-point to operation area is not always an option, and the instrumentation has to be flexible in order to conform to the tortuous lumens and cavities of the human body. Instruments with some form of flexibility are available, for example, catheters or flexible endoscopes. Although some of these instruments are steerable at the tip, they rely on the surrounding anatomy to support and guide their motion. Such guided motion can be very effective, a prime example being catheters guided through blood vessels. In other areas in the body, however, the anatomy can be too soft, e.g. in the colon, or too delicate, e.g. in the skull base, to deliver sufficient support and guidance (5). Self-guided instruments that can travel along multi-curved pathways while supporting their own weight and guiding their own motion can navigate through such soft or delicate areas, and have the potential to expand the reach of surgical procedures.

A special type of motion along multi-curved pathways is called Follow-the-Leader (FTL) motion, a term first coined in the field of snake-like robotics (6). This motion is comparable with the videogame "Snake", wherein the player steers the direction of the snake's head (the leader) while the snake's body automatically follows the created trajectory. A key characteristic of this motion is that it minimizes the required access, i.e. in an ideal situation the width of the curved pathway is equal to the width of the snake. FTL-motion is very beneficial for surgical practice as it enables

motion along complex pathways while minimizing the required access and in that way the invasiveness of the procedure (7).

### *1.1 State of the art*

FTL instruments found in literature developed for surgical purposes can be divided into two groups: shape-shifting instruments and telescoping instruments. Shape-shifting instruments contain a flexible shaft consisting of multiple steerable segments placed in series. FTL-motion is achieved by re-shaping the entire shaft to the shape of the path as the instrument moves forward, i.e. the shape of the shaft is shifted backwards along its body as the instrument moves forward as a whole. In telescoping instruments, the shaft consists of telescoping segments placed parallel to each other. Instead of moving the instrument forward as a whole, FTL-motion is now achieved by extending the tip of the shaft, while the rest of the shaft holds its position and shape.

Shape-shifting requires a serially segmented hyper-redundant shaft. These shafts are referred to as hyper-redundant as they contain (much) more degrees of freedom (DOFs) than strictly necessary for positioning their end-effector. FTL-motion is realized when each segment takes over the position and shape of the segment in front of it as the shaft moves forward. To achieve this, all segments have to be simultaneously actuated. In the literature, many experimental hyper-redundant shafts aimed for medical applications are described (7-29), a few of them employing FTL-motion with the group of Shigeo Hirose from Tokyo Institute of Technology already demonstrating it in 1988 (8-12). The actuators needed to realize the motion are either embedded in the shaft, referred to as intrinsic actuation, (11-20) or placed at the base of the instrument outside the shaft, referred to as extrinsic actuation (21-28). The common denominator for shape-shifting instruments is that all DOFs of the shaft must be simultaneously actuated to realize shape-shifting. As a consequence, shape-shifting instruments include at least one actuator for every DOF in their hyper-redundant shafts.

Telescoping instruments were also found in the literature (30-38). The concentric tube robots pioneered by the group of Robert Webster III at Vanderbilt University are the thinnest existing telescoping instruments, with outer diameters found in literature down to 2.39 mm (30). Concentric tube robots are based on a telescoping mechanism of concentric pre-curved tubes. By twisting and sliding the tubes relative to one another, the overall shape can be adjusted. As the movement of one tube affects the entire shape of the device, these instruments can only achieve FTL-motion over a limited set of specific paths (31, 39). As a solution Nguyen et al. proposed a hybrid steerable version wherein the tubes are cable-driven instead of pre-curved (36). This resulted in more control over the shape of the shaft, at the cost of a larger diameter (Ø6 mm). A more dexterous telescoping mechanism is the HARP (also called CardioArm, Ø10 mm) developed by Choset et al. and commercialized by Medrobotics into the Flex Robotic System (35, 40, 41). This system uses a telescoping mechanism of two concentric arms that alternate between flexible and rigid states. The arm that is made flexible is moved forward while guided by the arm that is made rigid in its curved shape. By alternating between the arms, the instrument moves forward as a whole. The concentric arms of the HARP are segmented structures that are rigidified by pressing the segments together. The interlaced continuum robot of Kang et al. introduces a continuous approach (33). In this robot, each arm consists of three flexible rods that are locked into shape by clamping mechanisms placed along the length of the shaft. The common denominator for telescoping instruments is that their parallel segments create a physical track that guides the next segment along the desired path.

### *1.2 Advantages and Disadvantages*

The current shape-shifting instruments incorporate an independent actuator for every individual DOF in their hyper-redundant shafts, providing independent control over every individual segment. However, FTL-motion in principle only requires a segment to copy the shape and position of its predecessor, making independent control over every segment not a necessity. As a

result, the current shape-shifting instruments require a level of control that is much higher than is strictly necessary for FTL-motion, leading to over-complex, expensive robotic systems.

Telescoping instruments use parallel segments to create a physical track that guides the next segment. The advantage as compared to shape-shifting instruments is that they require fewer actuators, and in this perspective a lower level of control. However, a disadvantage is that telescoping instruments rely on the relative change in stiffness between their parallel segments (5). In concentric tube robots, the stiffness and the curvature of the pre-bent tubes play a fundamental role in defining the path to be followed, limiting the robot to a restricted number of paths (42)Consequently, alternating the concentric arms between a flexible and rigid state, as in the HARP and the interlaced robot, limits the influence that the segments will have on each other at the price of a larger diameter.

### *1.3 Goal*

This paper explores a new concept for an FTL instrument that aims to combine the characteristics of shape-shifting and telescoping instruments. It is based on a **cable-driven hyper-redundant shaft** (adapted from shape-shifting instruments) that is **extrinsically** controlled via a **physical track** (adapted from telescoping instruments). In this way, the shaft does not require an independent actuator for each DOF, thus drastically reducing the required level of control and eliminating the need for computer-controlled actuation, while at the same time being suitable for a large variety of pathways not limited by the drawbacks of a telescopic device.

## 2 Mechanism Design

### *2.1 Mechanical FTL concept in 2D*

Figure 1a shows the 2D concept of our FTL instrument. The instrument contains a hyper-redundant shaft consisting of a series of jointed segments, each connected to a pair of cables. On the other side of the instrument, each pair of cables connect to one control-point. The vertical

movement of a control-point pulls one cable while releasing its antagonist. In this way, the vertical positions of the control-points translate to the angles of the segments and thus to the shape of the shaft.

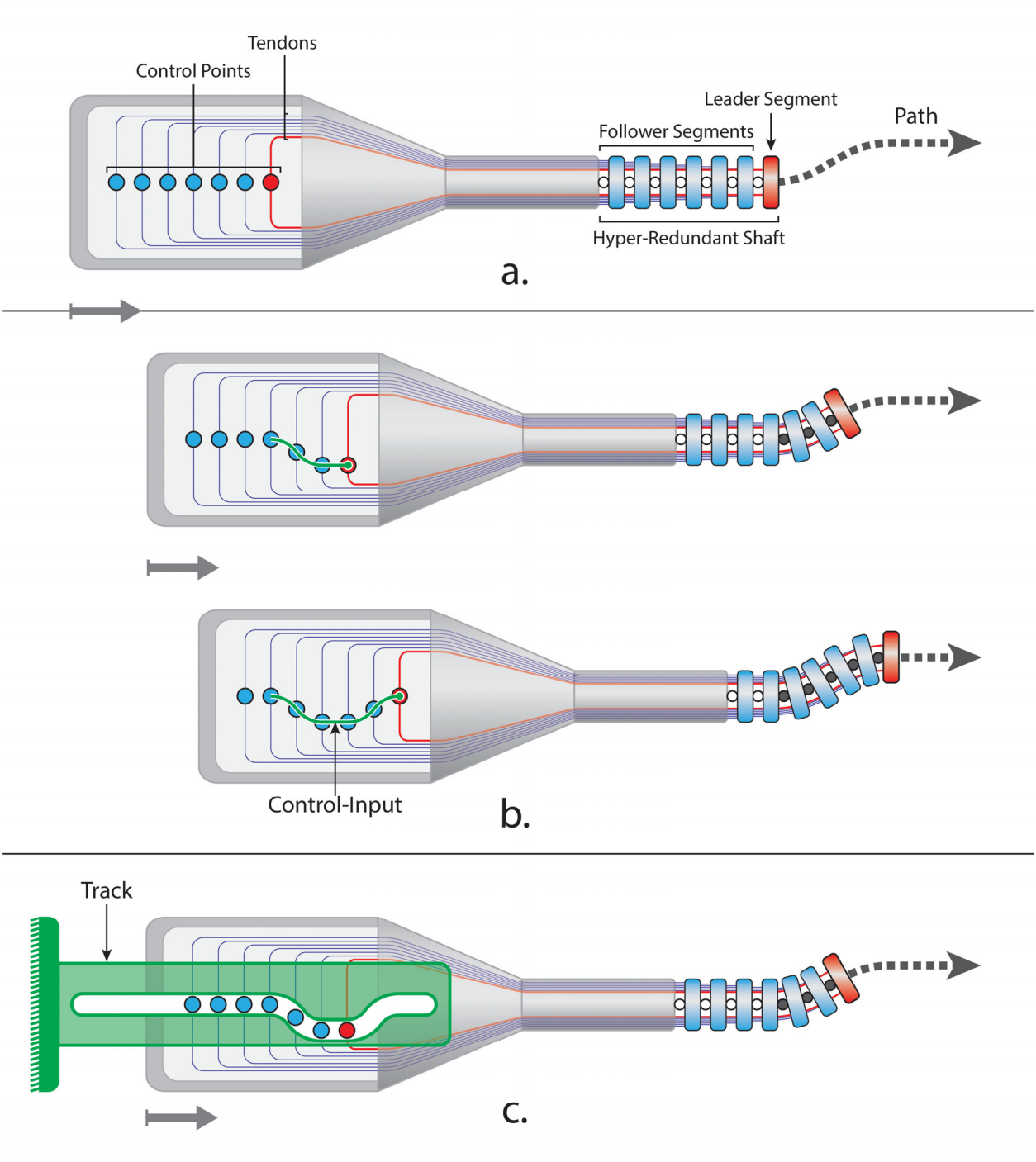


*Figure 1: 2D Concept of a Follow-the-Leader instrument. a) An instrument consisting of a cable-driven shaft. The vertical positions of the control-points determine the angles of the segments and thus the shape of the shaft. b) As the leader-segment follows the path,*

*the path of leading control-point (red) is outlined to visualize the control-input. Follow-the-Leader motion is achieved when the neighboring control-points follow the same control-input. c) A stationary track based on the control-input physically guides the control-points as the instrument moves forward, steering the shaft of the desired path.*

FTL-motion is characterized by the first segment of the shaft (the leader-segment, red in Figure 1a) tracing a path that is followed by the rest of the segments (the follower-segments, blue in Figure 1a). The leader-segment is controlled over the desired path by moving its "leading" control-point (red in Figure 1a) vertically while the instrument moves forward as a whole, as illustrated in the two steps of Figure 1b. As the motion continuous, the movement of the leading control point can be represented by a continuous line (green). This line is referred to as the control-input and represents all the vertical positions of the leading control-point as it travels along the desired path. Because the follower-segments are physically identical to the leader-segment, they will behave identically to the same control-input. Passing the control-input of the leader-segment to the follower-segments should therefore result in the follower-segments traveling along the same path as the leader-segment. FTL-motion can thus be achieved by passing the control-input of the leader-segment to the control-points of the follower-segments.

In mechanical terms, the control-input can be represented by a physical track, as visualized in Figure 1c, where the track contains a groove that encloses the control-points and is shaped in accordance with the control-input. In this configuration, the track remains stationary while the instrument moves forward. The track will guide the vertical movements of all control-points simultaneously, and in this way, FTL-motion can be achieved. The complex problem of controlling every cable of the hyper-redundant shaft individually is in this way reduced to a relatively simple cam-follower mechanism wherein all cables are controlled by a single physical track.

### *2.2 Mechanical FTL concept in 3D*

In the 2D concept of Figure 1c, all cables are controlled by a single track. As a result, antagonistic cables are connected to the same control-point, and these control-points are placed at the centerline of the instrument. As a consequence, the cables have to be redirected along 90 degrees bend before being connected to the control-points. From a mechanical perspective, redirecting

the cables, e.g. by pulleys or Bowden cables, will introduce friction within the system and/or increase its complexity. Redirecting cables can be avoided by rotating the track over 90 degrees as illustrated in Figure 2. With this solution, the track can no longer remain stationary while the instrument moves forward, but has to move downward along the now vertically placed set of control-points. Moreover, this configuration requires two tracks per plane instead of only one: one track controlling the upward motion and another track controlling the downward motion. The two tracks should be mirrored versions of each other so that one track pulls at a cable while the other track releases the antagonist cable over the same length. A 3D instrument should have a total of four such tracks to control the motion in the horizontal and vertical plane: two tracks for the motion in the horizontal plane and two tracks for the motion in the vertical plane.

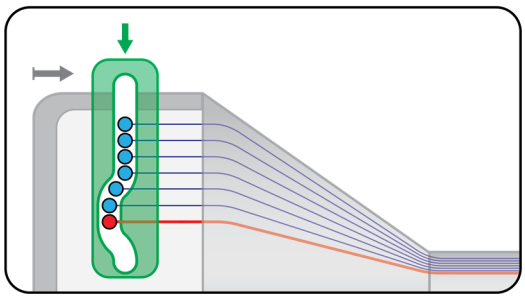

*Figure 2: Partial view of a Follow the Leader instrument showing a variant of the 2D concept of Figure 1c with the track rotated over 90 degrees.*

### *2.3 Cable configuration in the 3D shaft*

The hypothetical 2D shaft of Figure 1 should be converted to function in three dimensions. This results in a 3D shaft composed out of a bendable backbone that is divided into segments by solid disks. Four cables attach to each disk at 90 degrees intervals, providing independent control of the bending motion in the horizontal and vertical plane. Figure 3a shows such a hypothetical shaft in which the cables are placed in a circle and routed in a straight line along the circumference of the shaft. A drawback of this simple configuration is that it will not function in the concept of Figure 1c, because it is vital in this concept that the follower-segments behave identically to the leader-segment. The segments of Figure 3a do not behave identically to one another as their cables are not attached in the same horizontal and vertical plane. As a result, each segment will

bend in a plane that is slightly rotated as compared to the bending plane of its predecessor. Figure 3b shows a solution in which all cables are attached in the horizontal and vertical planes. This configuration requires the cables to be stacked, which will increase the shaft's diameter, making its miniaturization challenging. Figure 3c shows another solution in which the cables are routed along a helical path with a large pitch along the circumference of the shaft. All segments behave identically in this configuration as the cables are all attached in the same horizontal and vertical plane, with the advantage that the shaft can be easily miniaturized as all cables are routed along its circumference.

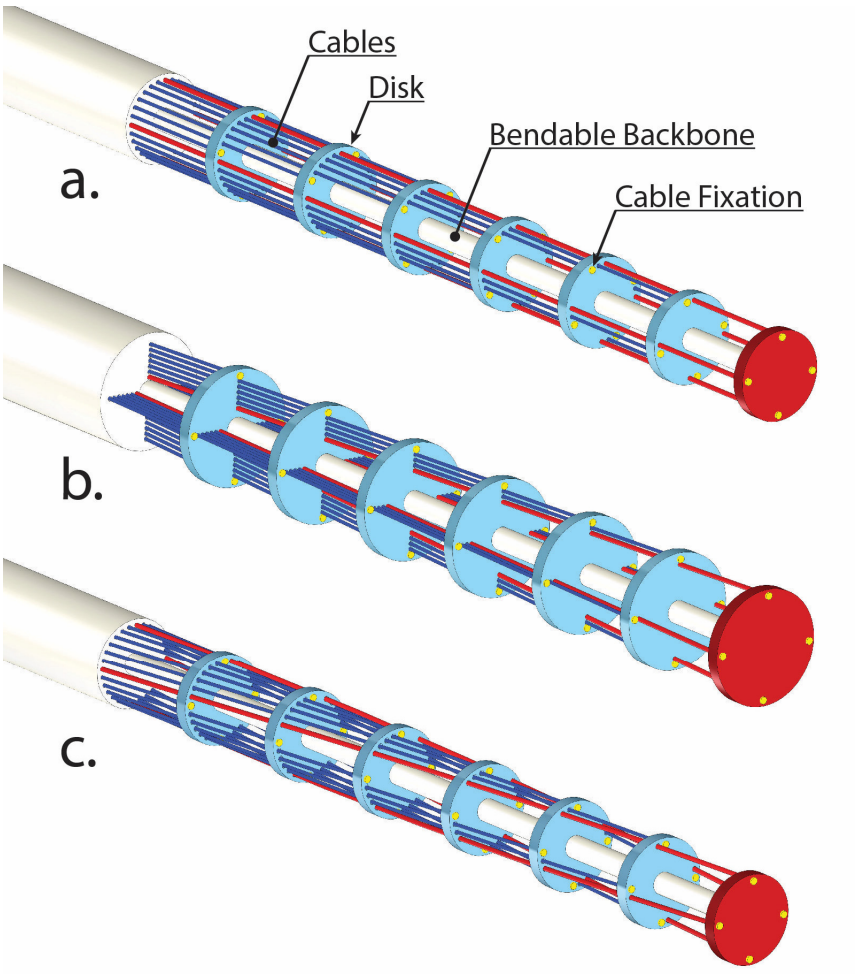


*Figure 3: Hypothetical shaft composed of a bendable backbone that is segmented by solid disks. a) Conventional cable-configuration. b) Cables fixated in the horizontal and vertical plane and stacked towards the centerline. c) Cables fixated in the horizontal and vertical plane and routed in a helical around the circumference of the shaft.*

## *2.4 Full 3D Concept*

The entire 3D instrument is schematically visualized in three stages in Figures 4a-c. Figure 4a shows the shaft and the cables, which are routed towards a larger diameter in the control-side of the instrument that contains a grooved cylinder, referred to as the revolver. Bars are positioned in the grooves of the revolver, allowing them to slide forward and backward. A cable connects to each bar so that the sliding of the bar pulls or releases the cable. The control-points are represented by blue ball-bearings that are fixed to each bar.

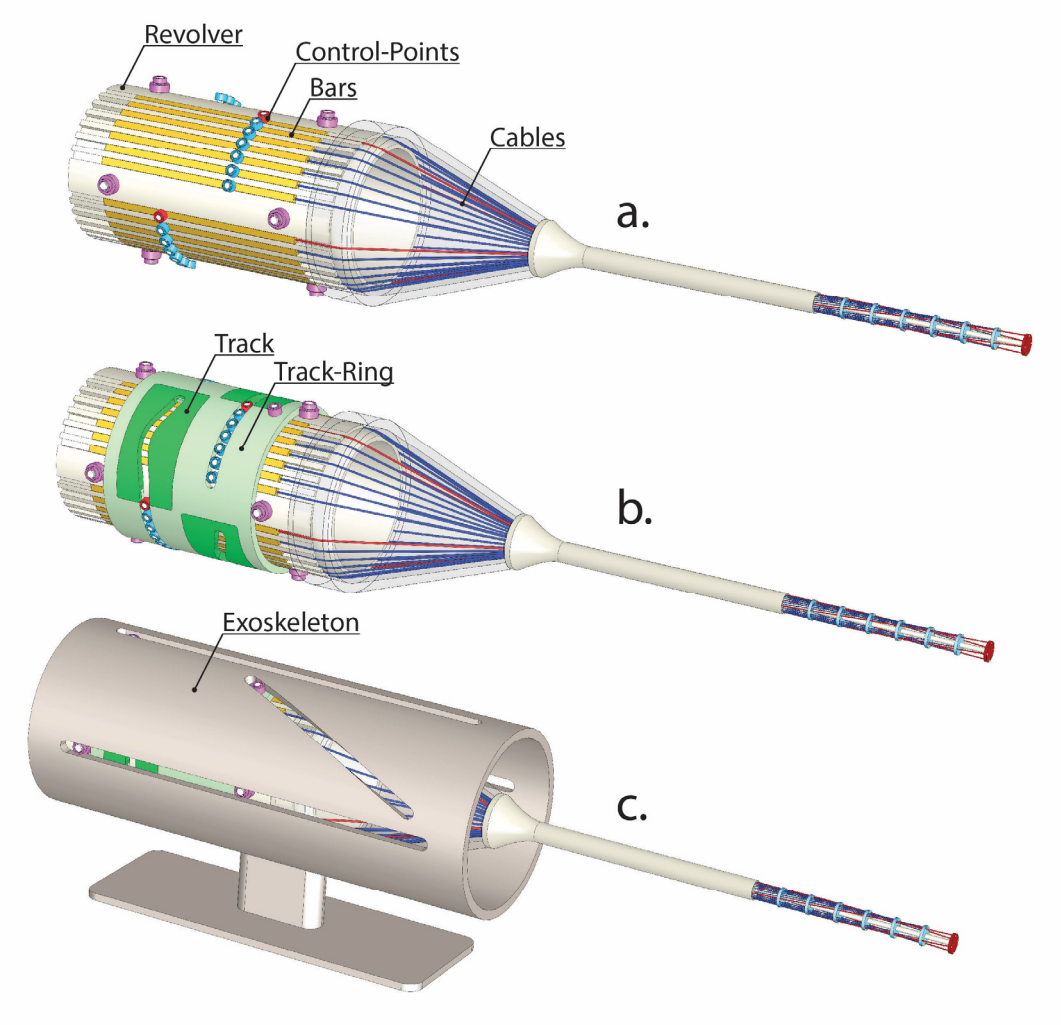


*Figure 4: Full 3D MemoFlex II instrument. a) The cables controlling the steerable segments of the shaft are connected to bars that slide over the revolver. Each bar has a control point integrated. b) A track-ring rotates around the revolver and the four integrated tracks*

*guide the control point over the path. An exoskeleton couples the steering and the forward/backward motion to achieve the FTL. Motion.*

The integration of the four tracks in the system is illustrated in Figure 4b. The tracks are held by a light green track-ring that can rotate around the revolver. The track-ring is fitted with straight grooves enclosing the ball-bearings in their initial configuration, holding them in a straight line so that the shaft is initially straight. The tracks, visualized in the dark green inserts, are fitted in line with these straight initial grooves. The mechanism works by rotating the track-ring as the instrument moves forward, resulting in the ball-bearings passing, one by one, from the straight initial groove to the curved groove of the track. During their rotation, the tracks will force the bars to move forward or backward, pulling or releasing the cables and causing the shaft to follow the pre-programmed track. Finally, Figure 4c shows how the rotation of the track-ring can be coupled to the forward and backward motion of the instrument. The instrument is suspended in a stationary exoskeleton containing four straight grooves and two helical grooves (only two straight grooves and one helical groove are visible in the figure). The straight grooves facilitate the forward and backward motion of the instruments while the track-ring is guided by the helical grooves, facilitating its rotation as the instrument moves forward or backward.

## 3. Experimental Setup

A Proof of Concept (PoC) prototype called MemoFlex II was developed based on the following criteria (Figure 5). The control side should be reusable, while the shaft and tracks were designed for disposable use.

The shaft is a continuous compliant structure that was 3D printed out of one single part from R5 photopolymer on a Perfactory® 4 Mini XL (EnvisionTec GmbH, Gladbeck, Germany) 3D printer, a close-up is given in Figure 5b. The shaft consists of a solid central backbone surrounded by segments built up from 3D printed helical structures. The backbone gives the shaft high axial stiffness, while the helical structure provides high torsion stiffness combined with low bending stiffness for easy bending of the segments. The cables are routed helically around the centerline

at an angle of 8 degrees and run through 3D printed holes at the circumference of the helical structures. In this way, the helical structures also serve as a guiding mechanism for guiding the cables smoothly along the bends. The shaft has a diameter of Ø8 mm, and each segment has a length of 12 mm. Four inner Ø1.2 mm channels run through the entire length of the shaft for use as lumens for insertion of additional instruments such as a gripper or suction tube. The maximum number of consecutive segments we managed to print was sixteen. For more detailed information about the shaft, we like to refer to (43).

Most of the control side components were machined out of aluminum. The bars were fabricated out of brass, creating low sliding friction with the aluminum revolver, and fitted with Ø4 mm ball bearings to serve as control-points. The diameter of the revolve should be minimized so to reduce the frictional forces the cables endure from their direction change in their path from the revolver to the shaft. A diameter of 88 mm was attained, which was determined based on the size of these ball bearings and the maximum number of sixteen segments we wanted to experiment with. A cone from acrylic material connects the shaft to the revolver, its transparency allowing for visual feedback during the assembly phase. The tracks were 3D printed to make them easy to replace.

In the MemoFlex II, one of the channels in the shaft was reserved for a Ø1.2 mm steel rod that is fixed to the stationary exoskeleton. This rod ensures that the segments that are not yet actively controlled are held in their initial straight position. The MemoFlex II is manually actuated via a rotation of a hand-crank. This pushes the revolver forward, while the helical grooves in the exoskeleton generate the appropriate rotation of the track-ring.

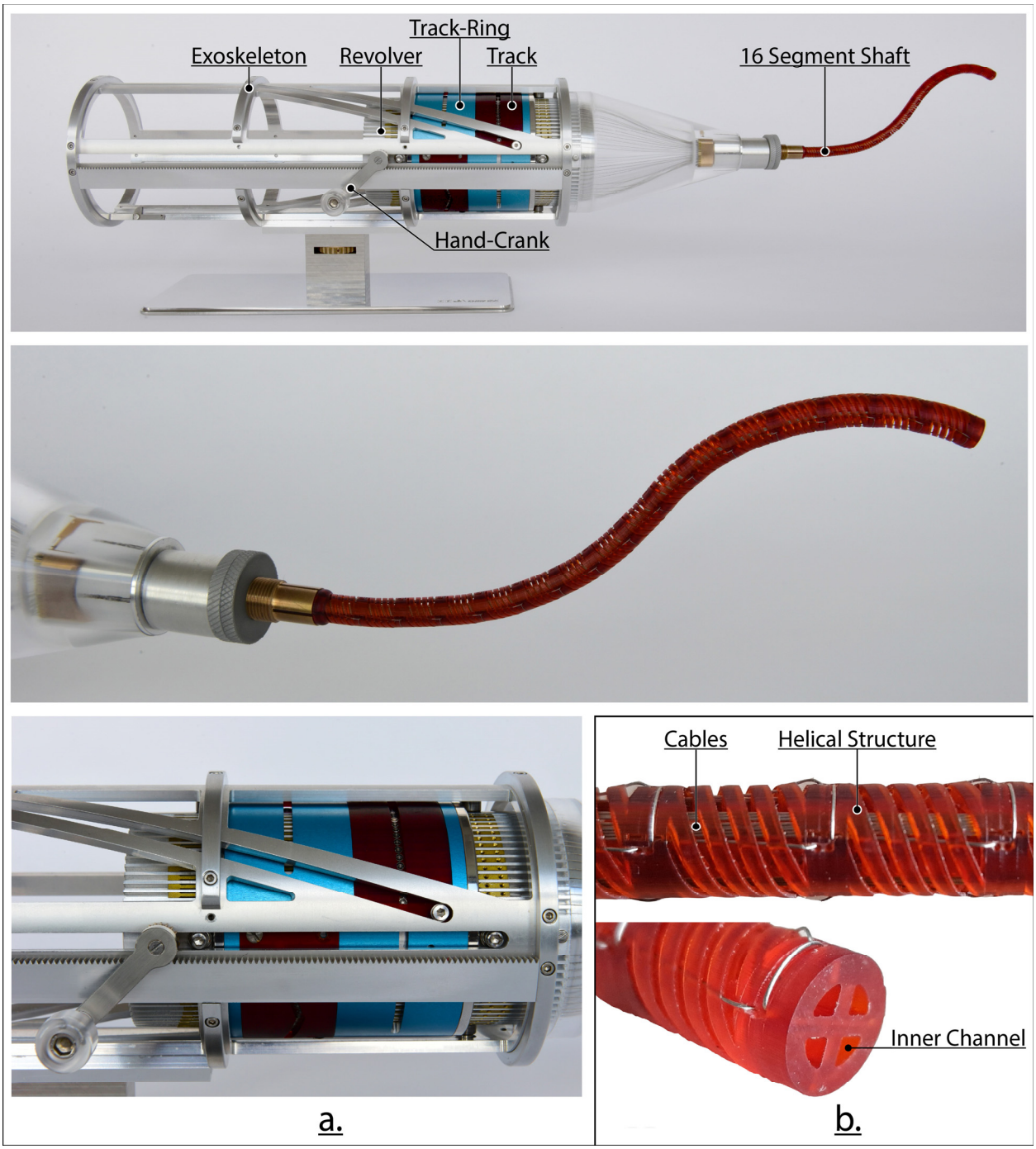


*Figure 5: Proof of Concept prototype MemoFlex II. a) From top to bottom, the MemoFlex II with a 16 segment shaft mounted, a close-up of the shaft, and a close-up of the revolver and track-ring within the exoskeleton. b) Close-up of the 3D-printed shaft.*

## *3.1 Reverse engineering the tracks*

In order to determine their required shape, the tracks were reverse engineered by shaping the shaft to a pre-described path and measuring the accompanying position of the cables. Four paths were chosen that were based on a shaft with seven segments and a total length of 84 mm (Figure 6a). A mold for each path was 3D-printed, providing a precisely fitting channel in which the shaft could be inserted (Figure 6b). Once the shaft was placed inside the mold, the accompanying elongation and shortening of the steering cables were registered by measuring the displacement of the corresponding bars inside the MemoFlex II. These measurements were conducted using image-processing. The bars were photographed and the displacement of each bar was measured by taking the length of each individual bar in the photo as reference, in this way errors due to projection were avoided. These displacement measurements were then used to configure the grooves in the tracks.

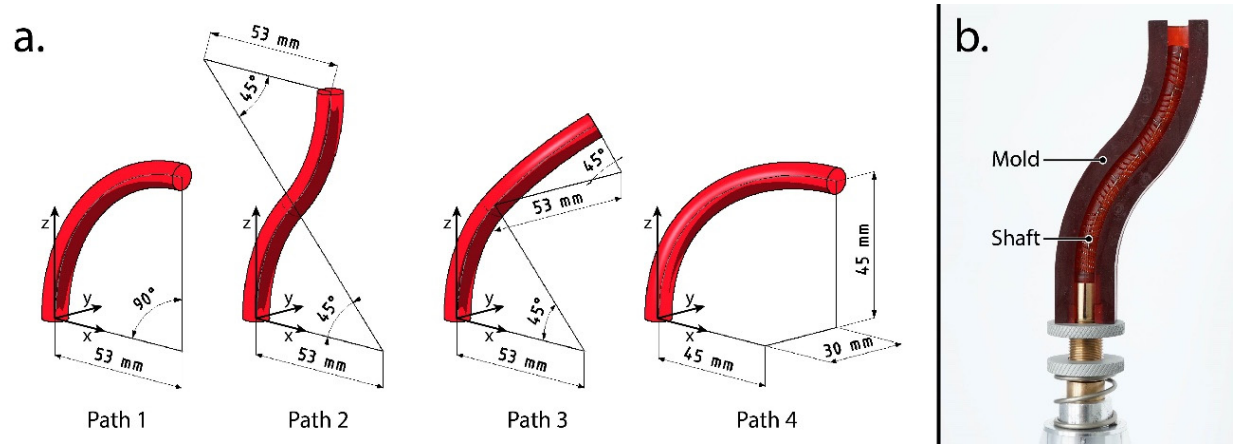


*Figure 6: Reverse engineering tracks based on molds of the path a) Paths 1 to 4. b) 7 Segment shaft inserted in the mold of Path 2.*

### *3.3 Experimental measurements*

The performance of the MemoFlex II was analyzed based on videos. As the shaft moved forward in the Z-direction, it was simultaneously filmed in both the horizontal X-plane and vertical Y-plane. Twelve consecutive video-frames were taken from each video and superimposed upon each other to form a single figure. This resulted in two figures per path, one showing the route of the shaft in the X-plane and the other showing the route of the shaft in the Y-plane. This way of presenting visualizes the footprint of the shaft, i.e. it shows how much space the shaft required during the

entire motion. Next, for each of the paths of Figure 6, the projections in the horizontal X- and vertical Y-planes were determined, representing the intended path in the ideal situation without position errors. The resulting ideal shaft contours were added to the figures as a reference to the intended paths. This helped visualize how well the shaft follows the intended path and reaches the desired end-position.

Two measurements were taken from these figures. As a first measurement, the maximum width of the footprint ($\Delta Wxz$ and $\Delta Wyz$) was derived. For perfect FTL-motion, the maximum width of the shaft's footprint is equal to its diameter. The maximum width of the footprint therefore provides a measure of how well the shaft is able to conform to the path traced by its tip, i.e. how well the MemoFlex II performs FTL-motion. Note that this measurement shows how well the shaft followed the route that was traced by its tip but provides no information on how well this route matches the intended path.

As a second measurement, the position error of the end-point of the shaft in its final position compared to the end-point of the reference contours was derived. This error was measured in 3D in each of the directions X, Y, and Z ($\Delta x$, $\Delta y$, and $\Delta z$). The spatial position error ($\Delta xyz$) was then calculated using:

$$\Delta xyz = \sqrt{\Delta x^2 + \Delta y^2 + \Delta z^2}. \qquad \textit{Eq. 1}$$

The spatial position error is a measure for the accuracy with which the MemoFlex II reached the desired end-position as specified by the pre-described paths of Figure 6.

## 4 Results

The MemoFlex II functions well, being capable of following a path in a fluent motion. Moreover, due to the continuous motion of its mechanism, there are no significant limitations on its forward velocity. Figure 7 shows the results of the reverse engineering method for all four paths. The footprint of the shaft can be seen through the superimposed consecutive video frames. The green

dashed lines represent the reference contours of the pre-described paths. The maximum footprints in the horizontal and vertical plane ($\Delta Wxz$ and $\Delta Wyz$) are denoted by arrows. The values for $\Delta y$ and $\Delta z$ were measured in the horizontal X-plane and the value of $\Delta x$ was measured in the vertical Y-plane. Table 1 shows the average values of the footprint and spatial position errors of all four paths together.

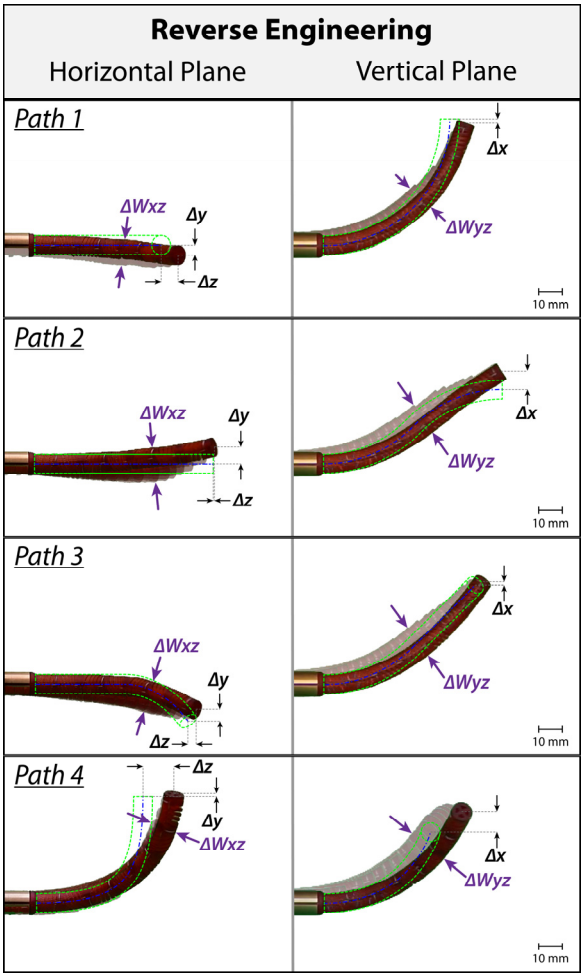


*Figure 7: Results for the reverse engineering method for a shaft with seven segments.* Δx, Δy, *and* Δz *represent the error measured in X, Y, and Z direction respectively.* ΔWxz and ΔWyz *represent the maximum footprint in the horizontal and vertical planes, respectively. The corresponding measurements are reported in Table 1.*

*Table 1: Measurements from Figure 7 in mm. ΔWxz and ΔWyz represent the average footprint in the horizontal and vertical planes for the four tracks in Figure 7. Δxyz is the root square of Δx, Δy, and Δz, and represents the position error of the shaft compared to the intended path.*

| | ***ΔWxz*** | ***ΔWyz*** | ***Δx*** | ***Δy*** | ***Δz*** | ***Δxyz*** |
|---|---|---|---|---|---|---|
| ***Path 1*** | 11,0 | 11,8 | 1,6 | 3,9 | 7,0 | 8,2 |
| ***Path 2*** | 15,0 | 13,8 | 8,1 | 7,1 | 0,5 | 10,7 |
| ***Path 3*** | 13,1 | 14,4 | 1,4 | 4,9 | 3,4 | 6,2 |
| ***Path 4*** | 11,3 | 17,1 | 8,8 | 1,4 | 12,8 | 15,6 |
| ***average*** | *12,6* | *14,3* | | | | *10,2* |

The results show that the MemoFlex II is capable of FTL-motion and that the reverse engineering method for configuring the tracks worked reasonably well. The average footprint of the Ø8 mm shaft in the horizontal and vertical planes was 12,6 mm and 14,3 mm, respectively. The average spatial position error was 10,2 mm.

## 5 Further optimization of the system

In general, the MemoFlex II appears to have more difficulties when following double-curved paths representing S-curves. Considering Path 2 in Figure 7, for example, the first curve of the path is followed reasonably well, while the second curve is damped and has almost no curvature. Another set of tracks was therefore constructed following a trial-and-error approach with the specific goal to improve on the performance of a double-curved path.

The trial and error approach started with a track-configuration that was similar to the reverse-engineered tracks of Path 2. This track configuration was then fine-tuned based on the reasoning that since the second curve appeared damped, the cables responsible for actuating that curve require more pulling. The part of the grooves in the tracks responsible for that pulling action was therefore made steeper. The performance of the resulting tracks was tested in the MemoFlex II, and another round of fine-tuning was performed to further optimize the behavior. This process of trial-and-error continued until the MemoFlex II followed a double-curved path of which the second curve matched the curvature of the first curve.

Figure 8a presents the results of the trial-and-error approach. The maximum width of the footprint ($\Delta Wxz$ and $\Delta Wyz$) was determined again. In contrast with Figure 7, the results of Figure 8 do not include a green reference contour, the reason being that the tracks were based on a trial-and-error approach and thus no specific pre-described path was used. Consequently, no spatial position error was calculated. Figure 8a shows that the first and second curves of the shaft do now approximately have an equal curvature in their final position.

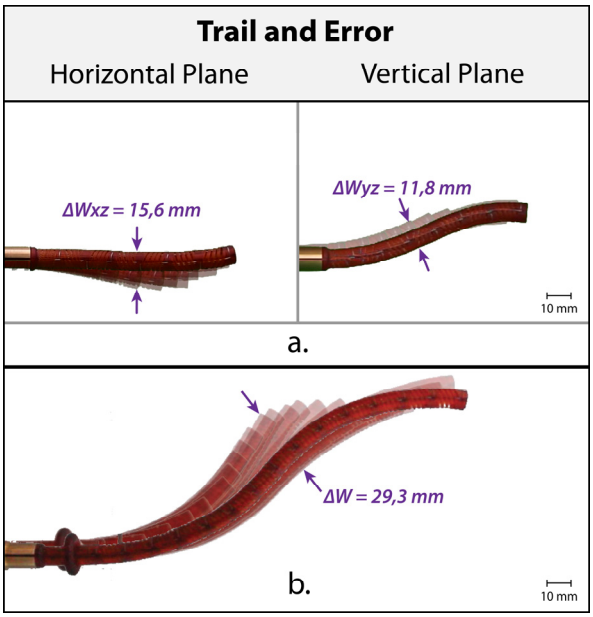


*Figure 8: Results from the S-shape tracks based on the trial and error approach. a) Shaft with seven segments on the horizontal and vertical planes. b) Shaft with 16 segments on the vertical plane.* ΔW *values are reported in the figure.*

In a final experiment, the MemoFlex II was fitted with a shaft with 16 segments. This shaft contains 32 DOF and a total of 64 steering cables, the maximum number of cables that can be controlled by the MemoFlex II. The diameter of the shaft remained Ø8 mm, and its total length reached 144 mm. The shaft was again given a double-curved path, which tracks were composed following the trial and error method. The result is given in Figure 8b. A maximum footprint ($\Delta W$) of 29,3 mm was measured.

## 6 Discussion

In this paper, we developed a fully mechanical Follow-the-Leader instrument based on a cable-driven hyper-redundant shaft that is extrinsically actuated by a physical track. In a previous attempt by our group, a similar approach was already explored (44). This resulted in a mechanism called the MemoFlex I that was based on a single 3D physical track and rigid-linked shaft. Splitting the track into four independent tracks and adapting a continuous shaft design, as was done in the MemoFlex II, significantly improved performance.

### *6.1 Performance*

Table 1 shows that the MemoFlex II performed better when following Path 1 that only contains a single curve, as compared to following Paths 2, 3, and 4 that contain multiple 2D or 3D curves. This is especially visible for Path 2 in Figure 7, of which the second curvature of the double-curved path is almost nonexistent. At first, one is tempted to explain this behavior through the play between the cables and its guiding components. Such play makes it possible for a cable to take the shortest route through the shaft, which reduces its effectivity for actuation. Yet, during the reverse engineering method, the cables run along the same routes and encounter the same play, meaning that this play was already incorporated in the design of the tracks. Another explanation can be found when considering the difference in cable tension during the reverse engineering method and the motion of the shaft. Due to the bending stiffness of the central backbone of the shaft, some force is required to bend it into shape. When applying the reverse engineering method, the shaft is forced into shape externally by the mold. During the motion itself, however, the shaft is forced into shape internally by the cables, leading to higher cable tensions, which will results in the cables stretching, shortening of the central backbone, and an in increase in cable friction. All of these effects work against the "preprogrammed" bending motion, resulting in flattened shaft curvatures. This effect is visible in the vertical plane of Path 1 of Figure 7, where the curvature of the shaft is lower than the curvature of the green reference contour. The effect is amplified when following a multi-curved path, like in the case of Path 2 were the two curves are

in opposite directions. The reason is that the cables that actuate the second curve are routed along the outside of the first curve. Because this first curve has a flattened curvature, the route is shorter than intended during the reverse engineering of the tracks, thus significantly reducing the effectiveness of the cables in actuating the second curve.

Another effect that influences the performance of the MemoFlex II is the cross-coupling between segments. As the shaft contains a compliant backbone that extends through all segments, a bending moment created in one segment will influence other more proximal segments. This effect is especially visible for the shaft with 16 segments in Figure 8b. When the tip of the shaft (Segment 1) changes direction to enter the second curve of the path, not only Segment 1, but the entire shaft moves a little bit in that direction. The cables of the more proximal segments should resist this movement and keep the segments straight, yet due to slack in the cables, play, and possible stretching of the cables, the shaft is still able to move. One of the major remaining issues is the stiffness of the shaft (43). In its current design, the shaft is not stiff enough to perform surgical tasks that require significant force. This is a downside compared to the alternating telescoping robots as these systems inherently include a stiffening mechanism in their design. Including a stiffening mechanism in the shaft of the MemoFlex II will challenge its miniaturization, as seen in the HARP and the interlace robot. If sufficient stiffness can be attained by for example pre-tensioning the actuation cables or integrating a stiffening mechanism inside the shaft will be a topic of future research.

### *6.2 An individual groove per cable*

Throughout this paper, FTL-motion was approached via a linear model, i.e. when all segments are identical, FTL-motion can be achieved by providing each segment with the same control-input. This led to the assumption that multiple cables could be controlled by a single groove. In reality, however, effects like cable stretching, cable friction, and cross-coupling between segments, introduce non-linearities. A way to compensate for these effects is to create a separate control input for each individual cable instead of using a shared control input for all cables simultaneously,

i.e. by controlling every cable by its own optimized groove. These grooves could, for example, be placed in series beside each other in the Track-Ring. For a shaft with seven segments and thus 14 DOF, this would require 28 individual grooves. Although changing from four to 28 control grooves sounds like a massive extension to the current system, in reality, this should not be that hard to incorporate, the reason being that, even though every groove will be individually optimized, the basic shape of the individual grooves will still be quite similar. This allows the grooves to be stacked close to one another, allowing for one track to support multiple grooves as shown in Figure 9. Such a configuration will only marginally extend the length of the revolver, while considerably increasing the level of control over the cables and enhancing overall performance.

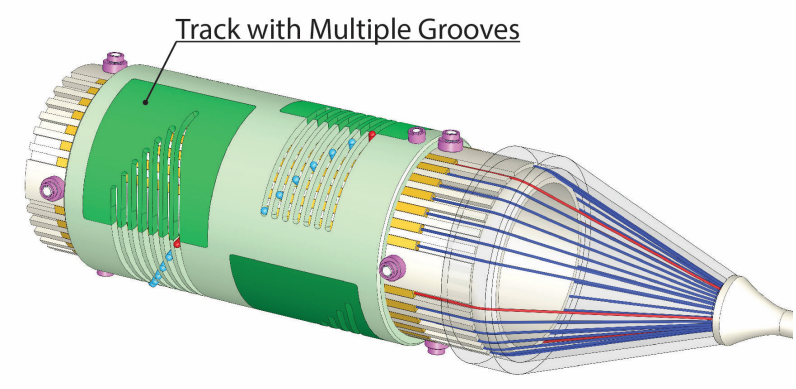


*Figure 9: Variation of Figure 4b, now including a track with an individual groove per cable. Integrating such a track would potentially improve the path following performance of the MemoFlex II.*

### *6.3 Model-based engineering of the tracks*

Our experiments have shown that the reverse engineering approach works, although it does not produce highly accurate results. Better results might be attainable by switching to a mechanical measuring method. None the less, we believe that the reverse engineering method is inherently flawed due to the early discussed difference in cable tension during the measurement and motion of the shaft. The trial-and-error approach increased the performance but is not a viable end solution as the iterative process is highly labor intensive. A better solution for configuring the tracks might be found by using a model-based approach for engineering the tracks. This would require a kinematic model the shaft that computes the required tension in the cables based on

the bending behavior of the shaft given its geometrical and material properties. From these computed cable tensions, the required positional changes of the cables could then be calculated, producing the required control input for each cable. Moreover, pre-determined control compensations, for example, considering the friction and/or play of the cables within the shaft could be included in the model. Engineering the tracks via a model-based approach would therefore complement the aforementioned hypothetical individual groove per cable setup. Future research will therefore be focused on model-based configuration of the tracks.

### *6.4 The MemoFlex II in a medical setting*

With its current dimensions and FTL capabilities, the MemoFlex II might already prove useful during surgeries that allow for a broad and relatively simple pathway, e.g. phonosurgery on the larynx while entering through the mouth. When the technique is sufficiently fine-tuned, operations that require more accurate performance and more challenging pathways, like endonasal surgery on the skull base, might also prove to be applicable cases. In these cases, we envision the physical tracks to be patient-specific, constructed via a model-based approach, and using pre-operative MRI or CT imaging to determine the most optimal path.

## 7 Conclusion

This paper introduced a novel concept for achieving a multi-curved Follow-the-Leader motion of a surgical instrument. The concept involves a cable-driven hyper-redundant shaft that is extrinsically controlled using a cam-follower mechanism based on physical tracks. By adopting this fully mechanical approach, no actuators were required. A prototype called MemoFlex II was developed to validate the proposed concept. It supports a Ø8 mm 3D-printed shaft with a modular setup to support a maximum of 32 DOFs. A Ø8 mm shaft with seven segments was able to follow predetermined multi-curved paths with a maximum footprint between 11,0 and 17,1 mm. In a future medical setting, we envision the MemoFlex II to function as a partly re-usable and partly

disposable device, wherein 3D-printing would allow for patient-specific tracks based on MRI or CT imaging and patient-specific shafts that are structurally optimized to suit the specific needs of individual MIS or NOTES procedures.

## 8 Funding Statement

This work is part of the VICI research program "Bio-Inspired Maneuverable Dendritic Devices for Minimally Invasive Surgery" with project number 12137, which is financed by the Netherlands Organization for Scientific Research (NWO).

## 9 Acknowledgements

Competing interests: None declared

Ethical approval: Not required

## 10 References

1. Atallah S, Martin-Perez B, Keller D, Burke J, Hunter L. Natural-orifice transluminal endoscopic surgery. The British journal of surgery. 2015;102(2):e73-92.
2. McLaughlin N, Eisenberg AA, Cohan P, Chaloner CB, Kelly DF. Value of endoscopy for maximizing tumor removal in endonasal transsphenoidal pituitary adenoma surgery. J Neurosurg. 2013;118(3):613-20.
3. Cavallo LM, Prevedello DM, Solari D, Gardner PA, Esposito F, Snyderman CH, et al. Extended endoscopic endonasal transsphenoidal approach for residual or recurrent craniopharyngiomas. J Neurosurg. 2009;111(3):578-89.
4. Cappabianca P, Cavallo LM, de Divitiis E. Endoscopic endonasal transsphenoidal surgery. Neurosurgery. 2004;55(4):933-40; discussion 40-1.
5. Loeve A, Breedveld P, Dankelman J. Scopes too flexible and too stiff. IEEE Pulse. 2010;1(3):26-41.
6. Choset H, Henning W. A Follow-the-Leader Approach to Serpentine Robot Motion Planning. Journal of Aerospace Engineering. 1999;12(2):65-73.
7. Burgner-Kahrs J, Rucker DC, Choset H. Continuum robots for medical applications: a survey. Ieee Transactions on Robotics. 2015;31(6):1261-80.
8. Ikuta K, Tsukamoto M, Hirose S, editors. Shape memory alloy servo actuator system with electric resistance feedback and application for active endoscope. Proceedings 1988 IEEE International Conference on Robotics and Automation; 1988 24-29 April 1988.
9. Buckingham R. Snake arm robots. Industrial Robot: the international journal of robotics research and application. 2002;29(3):242-5.
10. Palmer D, Cobos-Guzman S, Axinte D. Real-time method for tip following navigation of continuum snake arm robots. Robot Auton Syst. 2014;62(10):1478-85.

11. Son J, Cho CN, Kim KG, Chang TY, Jung H, Kim SC, et al. A novel semi-automatic snake robot for natural orifice transluminal endoscopic surgery: preclinical tests in animal and human cadaver models (with video). Surg Endosc. 2015;29(6):1643-7.
12. Tappe S, Yu D, Kotlarski J, Ortmaier T. Model reduction methods for optimal follow-the-leader movements of binary actuated, hyper-redundant robots. Mechanisms and Machine Science2018. p. 35-43.
13. Sars VD, Haliyo S, Szewczyk J. A practical approach to the design and control of active endoscopes. Mechatronics. 2010;20(2):251-64.
14. Tortora G, Dimitracopoulos A, Valdastri P, Menciassi A, Dario P, editors. Design of miniature modular in vivo robots for dedicated tasks in Minimally Invasive Surgery. 2011 IEEE/ASME International Conference on Advanced Intelligent Mechatronics (AIM); 2011 3-7 July 2011.
15. Rivas-Blanco I, Saz-Orozco Pd, García-Morales I, Muñoz V, editors. Robotic system for single incision laparoscopic surgery. IECON 2012 - 38th Annual Conference on IEEE Industrial Electronics Society; 2012 25-28 Oct. 2012.
16. Cepolina FE, Zoppi M. Design of multi-degrees-of-freedom dexterous modular arm instruments for minimally invasive surgery. Proceedings of the Institution of Mechanical Engineers, Part H: Journal of Engineering in Medicine. 2012;226(11):827-37.
17. Ho M, McMillan AB, Simard JM, Gullapalli R, Desai JP. Toward a Meso-Scale SMA-Actuated MRI-Compatible Neurosurgical Robot. IEEE Transactions on Robotics. 2012;28(1):213-22.
18. Clark J, Noonan DP, Vitiello V, Sodergren MH, Shang J, Payne CJ, et al. A novel flexible hyper-redundant surgical robot: prototype evaluation using a single incision flexible access pelvic application as a clinical exemplar. Surg Endosc. 2015;29(3):658-67.
19. Tzorakoleftherakis E, Mavrommati A, Tzes A. Design and Implementation of a Binary Redundant Manipulator With Cascaded Modules1. Journal of Mechanisms and Robotics. 2015;8(1):011002--10.
20. Berthet-Rayne P, Gras G, Leibrandt K, Wisanuvej P, Schmitz A, Seneci CA, et al. The i 2 Snake Robotic Platform for Endoscopic Surgery. Annals of Biomedical Engineering. 2018;46(10):1663-75.
21. Simaan N, editor Snake-Like Units Using Flexible Backbones and Actuation Redundancy for Enhanced Miniaturization. Proceedings of the 2005 IEEE International Conference on Robotics and Automation; 2005 18-22 April 2005.
22. Shang J, Noonan DP, Payne C, Clark J, Sodergren MH, Darzi A, et al., editors. An articulated universal joint based flexible access robot for minimally invasive surgery. Robotics and Automation (ICRA), 2011 IEEE International Conference on; 2011 9-13 May 2011.
23. He J, Liu R, Wang K, Shen H, editors. The mechanical design of snake-arm robot. IEEE 10th International Conference on Industrial Informatics; 2012 25-27 July 2012.
24. Reiter A, Bajo A, Iliopoulos K, Simaan N, Allen PK, editors. Learning-based configuration estimation of a multi-segment continuum robot. 2012 4th IEEE RAS & EMBS International Conference on Biomedical Robotics and Biomechatronics (BioRob); 2012 24-27 June 2012.
25. Li Z, Du R. Design and Analysis of a Bio-Inspired Wire-Driven Multi-Section Flexible Robot. International Journal of Advanced Robotic Systems. 2013;10(4):209.
26. Krieger YS, Roppenecker DB, Stolzenburg J, Lueth TC, editors. First step towards an automated designed Multi-Arm Snake-Like Robot for minimally invasive surgery. 2016 6th IEEE International Conference on Biomedical Robotics and Biomechatronics (BioRob); 2016 26-29 June 2016.
27. Evangeliou N, Tzes A, editors. A human-in-the-loop controlled shape memory alloy actuated robotic probe for minimally invasive surgical procedures. 2016 ELEKTRO; 2016 16-18 May 2016.
28. Ouyang B, Liu Y, Sun D, editors. Design and shape control of a three-section continuum robot. 2016 IEEE International Conference on Advanced Intelligent Mechatronics (AIM); 2016 12-15 July 2016.

29. Cianchetti M, Ranzani T, Gerboni G, Nanayakkara T, Althoefer K, Dasgupta P. Soft Robotics Technologies to Address Shortcomings in Today's Minimally Invasive Surgery: The STIFF-FLOP Approach2014. 122-31 p.
30. Webster Iii RJ, Romano JM, Cowan NJ. Mechanics of precurved-tube continuum robots. IEEE Transactions on Robotics. 2009;25(1):67-78.
31. Mahoney AW, Gilbert HB, III RJW. A REVIEW OF CONCENTRIC TUBE ROBOTS: MODELING, CONTROL, DESIGN, PLANNING, AND SENSING. The Encyclopedia of Medical Robotics. p. 181-202.
32. Gilbert HB, Rucker DC, Webster RJ, III. Concentric tube robots: The state of the art and future directions. Springer Tracts in Advanced Robotics2016. p. 253-69.
33. Kang B, Kojcev R, Sinibaldi E. The first interlaced continuum robot, devised to intrinsically follow the leader. PLoS ONE. 2016;11(2).
34. Amanov E, Granna J, Burgner-Kahrs J, editors. Toward improving path following motion: Hybrid continuum robot design. 2017 IEEE International Conference on Robotics and Automation (ICRA); 2017 29 May-3 June 2017.
35. Ota T, Degani A, Schwartzman D, Zubiate B, McGarvey J, Choset H, et al. A Highly Articulated Robotic Surgical System for Minimally Invasive Surgery. The Annals of Thoracic Surgery. 2009;87(4):1253-6.
36. Nguyen TD, Burgner-Kahrs J, editors. A tendon-driven continuum robot with extensible sections. Intelligent Robots and Systems (IROS), 2015 IEEE/RSJ International Conference on; 2015 Sept. 28 2015-Oct. 2 2015.
37. Conrad BL, Zinn MR. Interleaved Continuum-Rigid Manipulation: An Approach to Increase the Capability of Minimally Invasive Surgical Systems. IEEE/ASME Transactions on Mechatronics. 2017;22(1):29-40.
38. Li Z, Chengzhi S, Hongmin W, editors. Design and prototyping of a concentric wire-driven manipulator. 2016 6th IEEE International Conference on Biomedical Robotics and Biomechatronics (BioRob); 2016 26-29 June 2016.
39. Gilbert HB, Neimat J, Webster RJ. Concentric Tube Robots as Steerable Needles: Achieving Follow-the-Leader Deployment. IEEE Transactions on Robotics. 2015;31(2):246-58.
40. Johnson PJ, Rivera Serrano CM, Castro M, Kuenzler R, Choset H, Tully S, et al. Demonstration of transoral surgery in cadaveric specimens with the medrobotics flex system. Laryngoscope. 2013;123(5):1168-72.
41. Corporation M. website Flex Robotic System Raynham, Massachusetts: Medrobotics; 2019 [Available from: https://medrobotics.com.
42. Gilbert HB, Webster RJ, editors. Can concentric tube robots follow the leader? Proceedings - IEEE International Conference on Robotics and Automation; 2013.
43. Culmone C, Henselmans PWJ, van Starkenburg RIB, Breedveld P. Exploring non-assembly 3D printing for novel compliant surgical devices. PLOS ONE. 2020;15(5):e0232952.
44. Henselmans PWJ, Smit G, Breedveld P. Mechanical Follow-the-Leader motion of a hyper-redundant surgical instrument: Proof-of-concept prototype and first tests. Proceedings of the Institution of Mechanical Engineers, Part H: Journal of Engineering in Medicine. 2019;233(11):1141-50.